GEOPHYSICS, VOL. 74, NO. 5 (SEPTEMBER-OCTOBER 2009); P. E205–E214, 8 FIGS., 2 TABLES.
10.1190/1.3196240

Long-wavelength P-wave and S-wave propagation in jointed rock masses

Minsu Cha[1], Gye-Chun Cho[1], and J. Carlos Santamarina[2]

ABSTRACT

Field data suggest that stress level and joint condition affect shear-wave propagation in jointed rock masses. However, the study of long-wavelength propagation in a jointed rock mass is challenging in the laboratory, and limited data are available under controlled test conditions. Long-wavelength P-wave and S-wave propagation normal to joints, using an axially loaded jointed column device, reproduces a range of joint conditions. The effects of the normal stress, loading history, joint spacing, matched surface topography (i.e., joint roughness), joint cementation (e.g., after grouting), joint opening, and plasticity of the joint filling on the P-wave and S-wave velocities and on S-wave attenuation are notable. The ratio V_P/V_S in jointed rock masses differs from that found in homogeneous continua. The concept of Poisson's ratio as a function of V_P/V_S is unwarranted, and V_P/V_S can be interpreted in terms of jointed characteristics. Analytic models that consider stress-dependent stiffness and frictional loss in joints as well as stress-independent properties of intact rocks can model experimental observations properly and extract joint properties from rock-mass test data. Thus, joint properties and normal stress have a prevalent role in propagation velocity and attenuation in jointed rock masses.

INTRODUCTION

The mechanical characteristics and orientation of joints determine the small- and large-strain behavior of rock masses and various forms of conduction and diffusion properties (Priest, 1993; Guéguen and Palciauskas, 1994; Brady and Brown, 1995; Huang et al., 1995). In particular, although the state of stress has little effect on the stiffness of intact rock, it exerts a predominant effect on the stiffness and attenuation in jointed rock masses (Goodman, 1989; Zhao et al., 2006).

Rock-mass characterization with elastic waves presents important advantages for a wide range of applications, from infrastructure (e.g., rock slopes, foundations, and tunnels) to resource recovery and production (e.g., geothermal development, petroleum production, and waste isolation). However, data interpretation requires a proper understanding of the impact that rock-mass properties and the state of stress have on elastic-wave propagation parameters.

The elastic-wave velocity of jointed rocks has been described in terms of displacement-discontinuity models and effective-moduli models. Displacement-discontinuity models capture anisotropy, frequency-dependent amplitude, and phase, and they can accommodate joint conditions such as crack length and filling materials (Pyrak-Nolte et al., 1990a, 1990b; Boadu and Long, 1996; Yi et al., 1997). On the other hand, quasi-static effective-media models correspond to the long-wavelength regime, whereby the wavelength λ is much longer than the interjoint spacing S; this is the most common situation in seismology and exploration geophysics (White, 1983; Schoenberg and Muir, 1989; Schoenberg and Sayers, 1995). However, the study of long-wavelength propagation in a jointed rock mass is challenging in the laboratory, and data are limited.

The relation between engineering rock-mass properties, such as fracture frequency or rock-quality designation (RQD) and wave velocity, has been explored experimentally in the laboratory for P-waves (Sjogren et al., 1979; El-Naqa, 1996; Kahraman, 2001, 2002) and for P- and S-waves (Leucci and De Giorgi, 2006) and by means of analytic displacement-discontinuity models (Boadu, 1997). In general, these studies show a decrease in propagation velocity with increasing fracture roughness and frequency of joints, i.e., lower RQD. However, these investigations were conducted in the short-wavelength propagation regime or had no control on the effective normal stress, or both.

Fratta and Santamarina (2002) have developed a device to study long-wavelength S-wave propagation in a jointed rock column subjected to controlled normal stress conditions and explore the effect of joint thickness using clay gouge. We extend that study. First, we enhance the device and extend the test procedures to include P- and S-wave propagation. Second, we use higher normal stress levels to explore velocity-stress behaviors that might not manifest at lower normal stress levels (particularly in rough or cemented joints).

Manuscript received by the Editor 21 August 2008; revised manuscript received 14 April 2009; published online 3 September 2009.
[1]Korea Advanced Institute of Science and Technology (KAIST), Daejeon, Republic of Korea. E-mail: wwoofercha@hanmail.net; gyechun@kaist.edu.
[2]Georgia Institute of Technology, School of Civil and Environmental Engineering, Atlanta, Georgia, U.S.A. E-mail: jcs@gatech.edu.

Third, we use a wider range of block materials, block-surface roughness, joint spacing, joint cementation, and both clayey and sandy gouge. As in the Fratta and Santamarina (2002) study, we emphasize the stress normal to the joint plane. A description of the new device and a summary of the gathered data follow. Then, we analyze the results and present models that recover joint information from wave-propagation data.

EXPERIMENTAL STUDY: DEVICE AND MATERIALS

The device used to study the stress-dependent wave propagation characteristics in jointed rock masses consists of a stack of rock discs (Fratta and Santamarina, 2002). The cylindrical jointed rock column rests on a high-impedance steel base. A light metal cap is placed atop the rock column. The axial load hangs from the top cap by means of a 4-mm-diameter rod that runs along a central hole drilled in all discs; the rod-cap connection allows 3D rotation (Figure 1).

Shear-wave propagation

The propagation of torsional waves in columns is nondispersive, and the velocity is equal to the shear-wave velocity in an infinite medium with the same material characteristics (Kolsky, 1963). Furthermore, there is no geometric attenuation when waves propagate in a cylindrical column; hence, the measured attenuation is the intrinsic attenuation in infinite media. Following Fratta and Santamarina (2002), we take advantage of these observations to determine the shear-wave propagation parameters from the first torsional resonant mode of the column. Figure 1a shows a sketch of the jointed rock column with the peripheral electronic devices used to monitor the torsional resonance. Two accelerometers are mounted on the top cap at diametrically opposite locations, aligned normal to the radius to detect any torsional motion.

Torsional excitation is created by suddenly releasing the column from a quasi-static deformation enforced at the top of the column, thereby allowing the column to vibrate freely. The global strain was kept below $\gamma = 10^{-6}$ in all tests (joint strain $<10^{-5}$). The signals from the two accelerometers include flexural and torsional motions. The flexural response of the long column is a lower-frequency component that can be filtered (during measurements or postprocessing) or cancelled by subtracting the time series gathered with the two diametrically opposite accelerometers (Figure 1a; typical signals and data reduction details in Fratta and Santamarina, 2002). The signal is then transformed to the frequency domain to obtain the resonance spectrum of the torsional shear response.

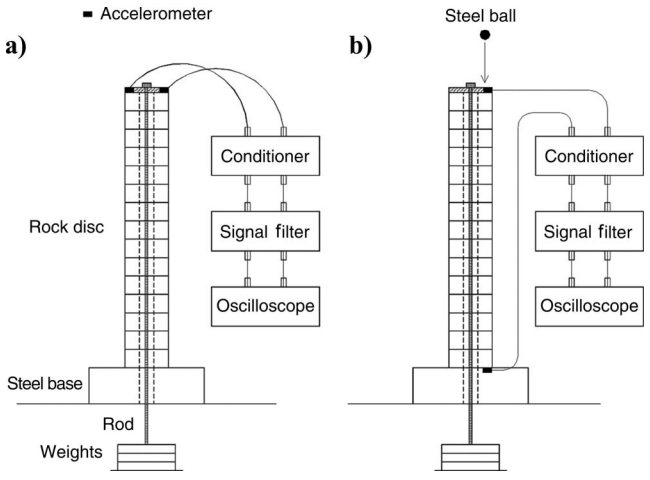

Figure 1. Stress-controlled jointed rock column. Peripheral electronic devices for (a) S-wave (resonance) and (b) P-wave (pulse) propagation studies.

The resonant frequency f_n and the damping ratio D are recovered from the resonance spectrum. For the given boundary conditions, the column vibrates as a free/fixed system, i.e., free at the top and fixed at the bottom. The corresponding wavelength λ for first-mode resonance is four times the column length L. Hence, the torsional shear-wave velocity is $V_S = 4Lf_n$. The damping ratio D, the attenuation α_D, and the quality factor Q are related as $D = \alpha_D\lambda/2\pi = 1/2Q$ for low-loss conditions. The attenuation $\alpha_D[1/\mathrm{m}]$ therefore can be computed readily by using D measured from the resonance spectrum.

Longitudinal-wave propagation

The presence of the rod and weights affects longitudinal resonance, and the column cannot be considered a free/fixed system in longitudinal vibration. Instead, we measure the longitudinal-wave velocity using two accelerometers aligned in the vertical direction, one mounted at the top of the column and the other on the lower face of the bottom disk, next to the central orifice. Figure 1b shows the instrumentation and peripheral electronic devices used to monitor the longitudinal-wave propagation.

The column is excited by the impact of a small steel ball dropped from a constant height; the global strain level ε is less than 10^{-5} for all the applied normal-stress levels (joint strain $<10^{-4}$). The longitudinal-wave velocity is computed as $V_P = L/\Delta t$, where Δt is the traveltime. A reliable determination of P-wave attenuation is impossible with this test procedure.

Longitudinal-wave propagation is dispersive in columns because radial inertia adds to longitudinal inertial effects. The asymptotic approximation for the long-wavelength phase velocity is

$$V_{\mathrm{ph}} = \sqrt{\frac{E}{\rho}}\left[1 - \pi^2\nu^2\left(\frac{r}{\lambda}\right)^2\right] \qquad (1)$$

for $r/\lambda < 0.1$ in terms of Young's modulus E, mass density ρ, Poisson's ratio ν, and the radius of the rod r (Rayleigh-Pochhammer; see Kolsky, 1963). The propagation velocity and the central frequency of the received signal are used to estimate the wavelength, which remains at about $\lambda \approx 0.7L$ in all tests. Accordingly, the anticipated geometric dispersion is less than 2%, which is below the measurement error (refer to Table 1 for the dimensions of the stacks of discs).

Long-wavelength condition

The group velocity in periodic discrete media is a function of the ratio between λ and the internal spatial scale of the medium, which in this case is the joint spacing S. If the velocity for an infinite wavelength is V^∞, then the group velocity V_g^λ for wavelength λ can be estimated as (Brillouin, 1946)

$$V_g^\lambda = V^\infty \cos\left(\frac{\pi S}{\lambda}\right) \qquad (2)$$

for $\lambda \geq 2S$, where S is the interjoint spacing. Note that the particle motion in two consecutive disks is completely out-of-phase when λ

$= 2S$ (i.e., π shift; Figure 2). In this case, the restitution force is maximum and the discrete medium hinders wave propagation — hence the name *cutoff wavelength*. Thus, the jointed rock mass acts as a low-pass filter, and the group velocity decreases as λ approaches the internal length scale S.

Figure 2 presents experimental results that confirm these observations. Jointed rock columns were formed with different numbers of gneiss discs and clean joint conditions (column lengths: 3, 5, 7, 9, 11, 13, and 15 disks). Torsional excitation values were gathered at three normal stress conditions (σ of 37, 149, and 445 kPa). The three trends confirm asymptotic shear-wave velocity values when the columns consist of approximately nine or more disks.

Because of the results shown in Figure 2, the following measurements were performed on columns with at least 13 discs (Table 1), so the column length is $L \geq 13S$ for an interjoint spacing of S. In torsional resonance, $\lambda = 4L$, the wavelength-to-spacing ratio is $\lambda/S \geq 52$, and the error in the group velocity is less than 0.2% according to equation 2. In the case of longitudinal propagation, the wavelength for the central frequency is typically $\lambda \sim 0.7L = 10S$, and the error in the group velocity is about 5% (limited experimental data with columns of 11 and 15 discs show a variation in the P-wave velocity lower than 7%.) On the basis of this analysis and experimental results, we conclude that the long-wavelength condition ($\lambda/S \gg 2$) sought in this study is adequately satisfied.

Tested rocks and joints

A total of 24 different disc-joint conditions were tested to explore the effect of the disc thickness T, the disc surface topography or joint roughness, the presence of gouge material, the loading history, and the joint cementation (e.g., after grouting). Table 1 summarizes the properties of the discs used to investigate these variables; the tested joint-disc combinations are listed in Table 2.

The interjoint spacing S is equal to the intact rock thickness T plus the joint thickness t, that is, $S = T + t$. We studied the effect of T using different disc thicknesses. In addition, we simulated the presence of gouge material in joints by adding clean, uniform sand (with a mean particle size of 0.2 mm) or a kaolinite paste between the discs when the jointed rock column was assembled.

Surface topography tests were designed to study the effect of clean, grooved, slickensided surfaces (rather than mismatched rough surfaces). Dental gypsum discs were cast on metal molds that had been machined in one direction to attain the transverse profiles created by Barton and Choubey (1977) for a joint roughness coefficient (JRC) of zero or planar, 6–8, 12–14, and 18–20 (Figure 3). A complete set of 15 discs was created for each topography. When the discs were stacked, the surfaces of the contiguous discs matched very closely.

The study of cemented joints was conducted by cementing gypsum discs sequentially, first in groups of two discs and then in groups of 4, 8, and 16 discs. The last case implies that all joints in the column are bonded together. The role of joint bonding gains relevance for geologic healing effects as well as in grouting of rock masses for engineering applications.

Each column was first subjected to staged loading to the desired maximum normal stress (400–700 kPa) and then was subjected to

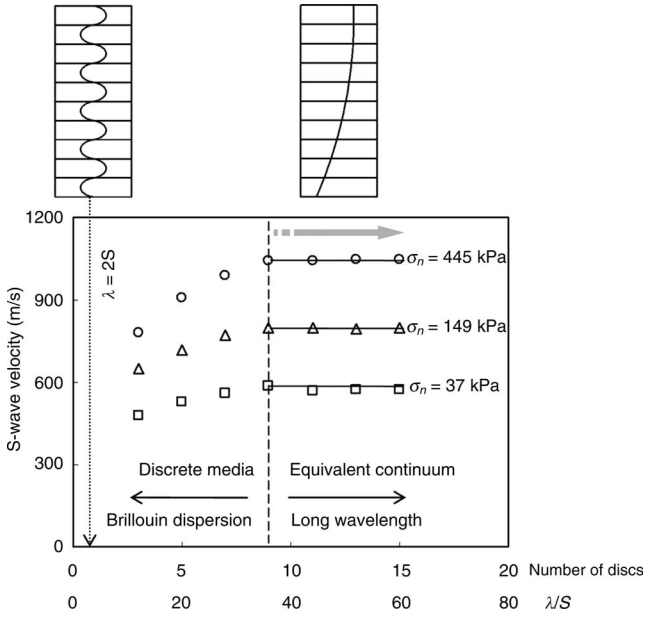

Figure 2. Wavelength-to-joint spacing ratio, inherent low-pass filter effect. Shear-wave velocity is a function of λ/S. Data were gathered with gneiss blocks and clean joints.

Table 1. Properties of materials used to make the discs. Data in parentheses are for gypsum.

Disc material	Gneiss	Acetal	Dental gypsum[a] (gypsum[b])
Dimensions	$T = 25.4$ mm	$T = 20, 25, 30$ mm	$T = 25$ mm
	ID = 25 mm	ID = 25 mm	ID = 25 mm
	OD = 63.2 mm	OD = 60 mm	OD = 52.6 mm
Preparation	Discs: from NX core	Discs: from rod	Discs: cast in molds
	Hole: water jet	Hole: milling machine	
	Cut: diamond saw and polished	Cut: milling machine	Surface: machined 1D roughness profile
	Surface: smooth	Surface: smooth	
Density ρ	2704 kg/m^3	1410 kg/m^3	1690 (847) kg/m^3
Intact V_S	3100 m/s	970 m/s	2070 (1270) m/s
Intact V_P	4750 m/s	2310 m/s	3250 (1920) m/s
Number of discs in column	15	13	15 (16)

[a]Water/gypsum ratio = 1:3. Dental gypsum is a high-stiffness casting material used in dental applications (material source: Maruishi Plaster Co., Ltd.)
[b]Water/gypsum ratio = 1:1. T = disc thickness; ID = inside diameter; OD = outside diameter

staged unloading. We determined the P- and S-wave propagation parameters at each stress stage.

EXPERIMENTAL RESULTS

Velocity

The P- and S-wave velocity data are plotted as a function of normal stress in Figures 4 and 5 for all joint conditions to compare the effects of (a) joint spacing in the case of clean joints, (b) joint roughness, (c and d) joint filling, (e) stress history, and (f) joint bonding (for S-waves only). Data points in these figures indicate experimental results, whereas lines correspond to the fitted analytic model trends, discussed in the next section.

Observations related to the effect of different joint conditions on propagation velocity follow. Unless noted, these observations apply to V_P and V_S.

State of stress (Figures 4 and 5). — The P- and S-wave propagation velocities increase as the normal stress increases for all joint conditions, rock materials, and joint spacing. This stress-dependent sensitivity of jointed rock masses contrasts with the stress-independent stiffness of the material that makes the blocks.

Joint spacing (Figures 4a and 5a). — The wave velocity increases as the joint spacing $S = T + t$ increases. The softening effect of joints on the column stiffness diminishes.

Roughness — no gouge material (Figures 4b and 5b). — The smoother the surface, the lower the propagation velocity at low normal stress and the higher the stress sensitivity (Kahraman, 2002). Therefore, the V-σ trends tend to converge as the normal stress σ increases. All experimental evidence shows that well-matched grooved surfaces exhibit the highest stiffness within the normal stress range explored here. However, if roughness purposely is mis-

Table 2. Summary of test conditions.

Test	Purpose	Disc	Gouge	Condition	Figure		
					V_P	V_S	D_{rm}
1	Disc thickness	Acetal	None	$T = 20$ mm	4a	5a	6a
2				$T = 25$ mm			
3				$T = 30$ mm			
4	Surface roughness	Dental gypsum	None	JRC ≈ 0	4b	5b	6b
5				JRC = 6–8			
6				JRC = 12–14			
7				JRC = 18–20			
8				Mismatched			
9	Gouge (coarse)	Gneiss	Sand	Clean	4c	5c	6c
10				$t = 1.0$ mm			
11				$t = 1.5$ mm			
12	Gouge (fine)	Gneiss	Clay	Clean	4d	5d	6d
13				$t = 0.5$ mm			
14				$t = 1.0$ mm			
15				$t = 1.5$ mm			
16	Loading history	Gneiss	None	Loading	4e	5e	6e
17				Unloading			
18			Clay	Loading			
19				Unloading			
20	Joint cementation[a]	Gypsum (planar)	None	$L_{bond} = 40$ cm	—	5f	6f
21				$L_{bond} = 20$ cm			
22				$L_{bond} = 10$ cm			
23				$L_{bond} = 5$ cm			
24				$L_{bond} = 2.5$ cm			

[a]The bonded length L_{bond} corresponds to the number of discs per cemented block: 2.5 cm = 1 disc; 5 cm = 2 discs; 10 cm = 4 discs; 20 cm = 8 discs; 40 cm = all joints.

T = disc thickness, JRC = joint roughness coefficient, t = gouge thickness, L_{bond} = bonded length, V_P = P-wave velocity, V_S = S-wave velocity, D_{rm} = S-wave damping ratio.

matched when consecutive disks are rotated by $\pi/2$, then the column of mismatched surface topography has the lowest stiffness (Figure 5b; P-wave data were not gathered in this test).

Joints filled with gouge material (Figures 4c and d, 5c, and d). — The P-wave and S-wave velocities decrease and the stress dependency increases as the joint-filling thickness increases. Both effects are more pronounced in the presence of clay than in the case of nonplastic gouge material. A very thin layer of a material with low shear modulus could have a pronounced impact on V_S yet a limited effect on V_P; a thin water film would be an extreme case. This is highlighted by the data gathered with a 0.5-mm clay layer in Figures 4d and 5d (there is even a minor increase in V_P, suggesting enhanced transmission of longitudinal motion).

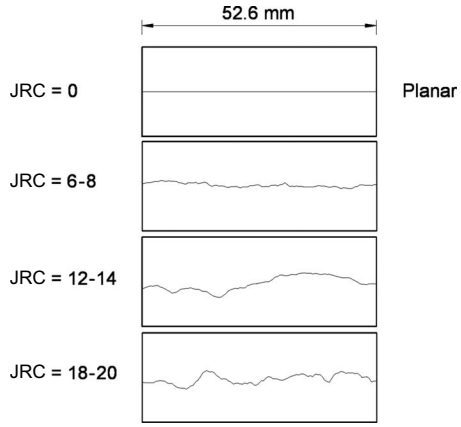

Figure 3. Selected roughness profiles (horizontally scaled to 53/100).

Load history (Figures 4e and 5e). — The wave velocity in jointed rocks reveals that the rock mass retains memory of the loading history. At a given normal stress, the wave velocity is higher during unloading than during loading in clean rough joints and in planar joints with gouge material (the stiffening of joints caused by preloading tends to vanish in clean planar joints). Load history effects suggest changes in asperities on the faces of joints and in the gouge material. In Figure 4e, the P-wave velocity is slightly lower during unloading for the case of clean joints; this could result from measurement bias (unidentified cause) or from surface damage in the gneiss discs during loading (yet there was no visual evidence of damage).

Cemented joints (S-wave data in Figure 5f. — P-wave data were not gathered in this test). Joint bonding increases shear-wave velocity through the rock mass and decreases its stress sensitivity. Eventually, the fully cemented rock mass exhibits a high shear-wave velocity (see also the field data in Kikuchi et al. [1997]) and the response becomes stress independent.

Damping

Values for damping ratio D are plotted in Figure 6. The main observations from these data include the following.

- *State of stress (Figure 6a-f):* In all cases, the damping ratio decreases as the normal stress increases.
- *Joint spacing*: Joint spacing has no measurable influence on damping (Figure 6a), which suggests the rock-mass damping is controlled mainly by losses in joints.
- *Roughness — no gouge material (Figure 6b):* There are fewer losses in matched grooved joints than in planar surfaces.

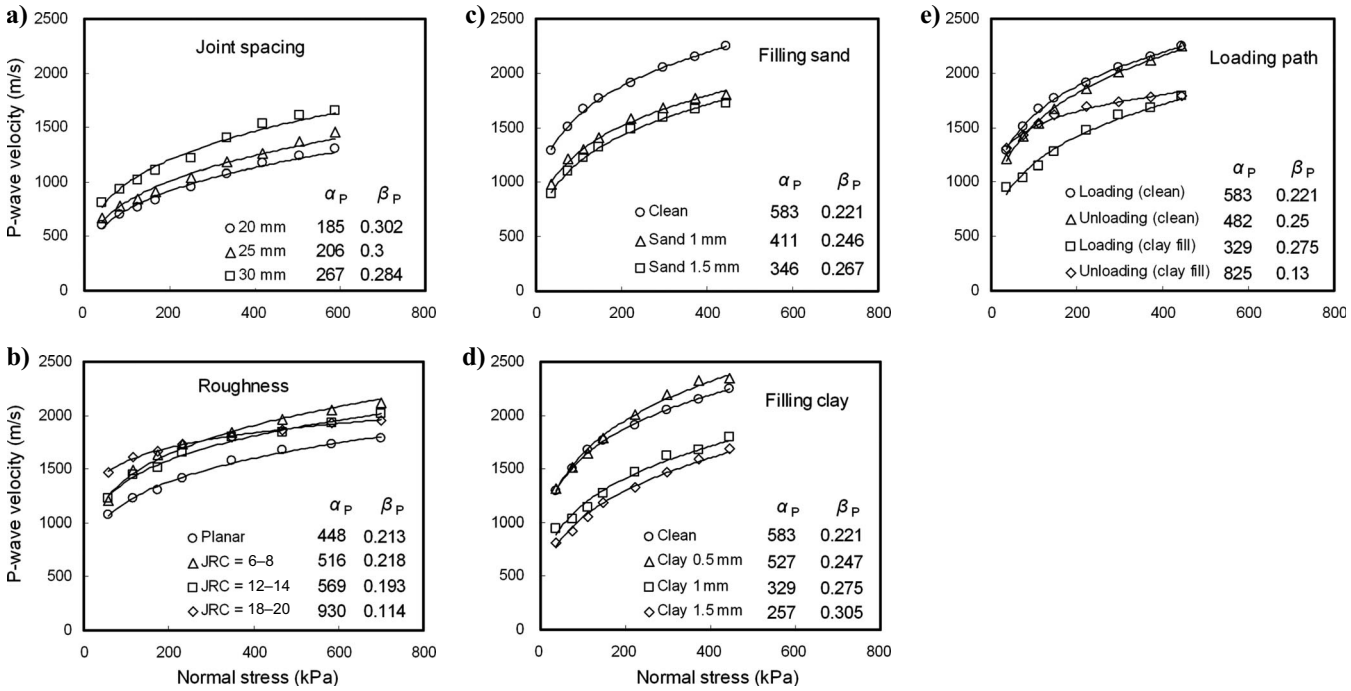

Figure 4. P-wave velocity V_P for different rock-mass conditions and stress levels: (a) effect of joint spacing (13 acetal discs, clean joints), (b) effect of joint roughness (15 dental gypsum discs), (c, d) effect of joint fillings (15 gneiss discs), and (e) loading and unloading path (15 gneiss discs). Higher JRC value corresponds to rougher surfaces. "Sand 1 mm" stands for 1-mm-thick sand filling. The values for α_p (m/s) and β_p are the rock-mass wave parameters in equation 3.

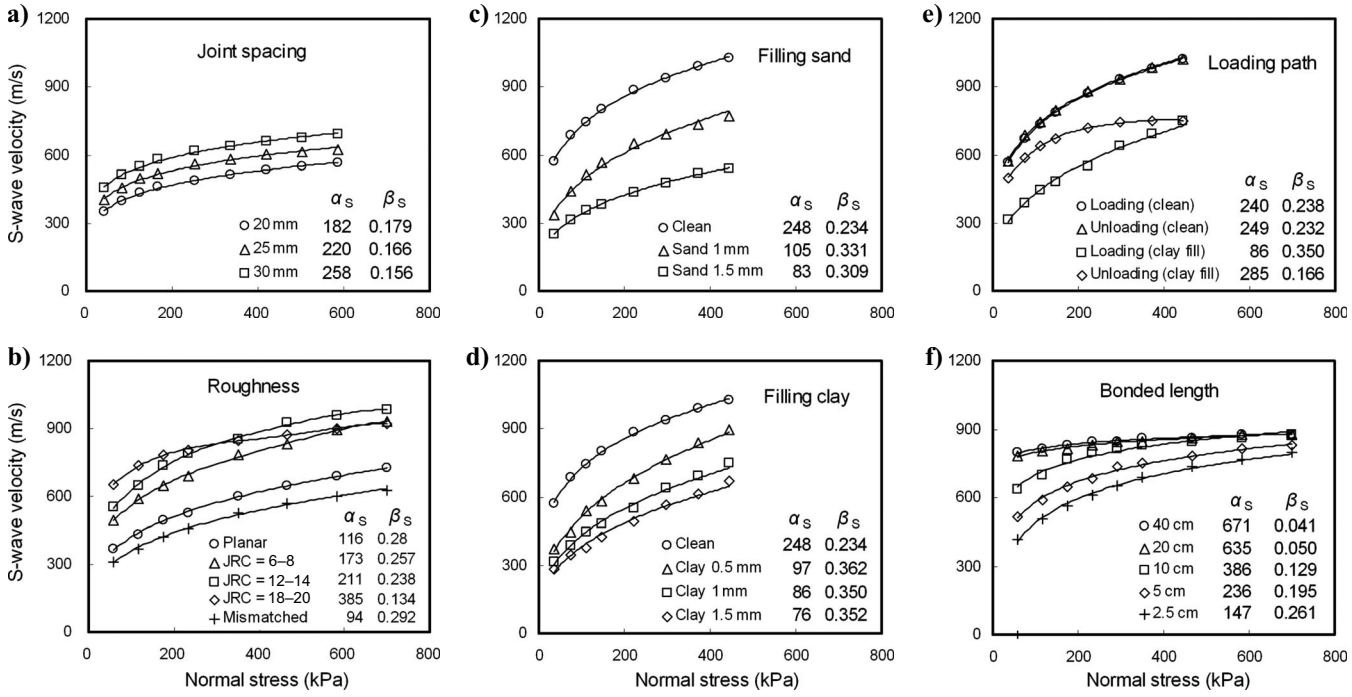

Figure 5. S-wave velocity V_S for different rock-mass conditions and stress levels: (a) effect of joint spacing (13 acetal discs, clean joints), (b) effect of joint roughness (15 dental gypsum discs), (c, d) effect of joint fillings (15 gneiss discs), (e) loading and unloading path (15 gneiss discs), and (f) effect of joint cementation (16 gypsum discs). The higher JRC value corresponds to rougher surfaces. "Sand 1 mm" stands for 1-mm-thick sand filling. The values for α_s (m/s) and β_s are the rock-mass wave parameters in equation 3.

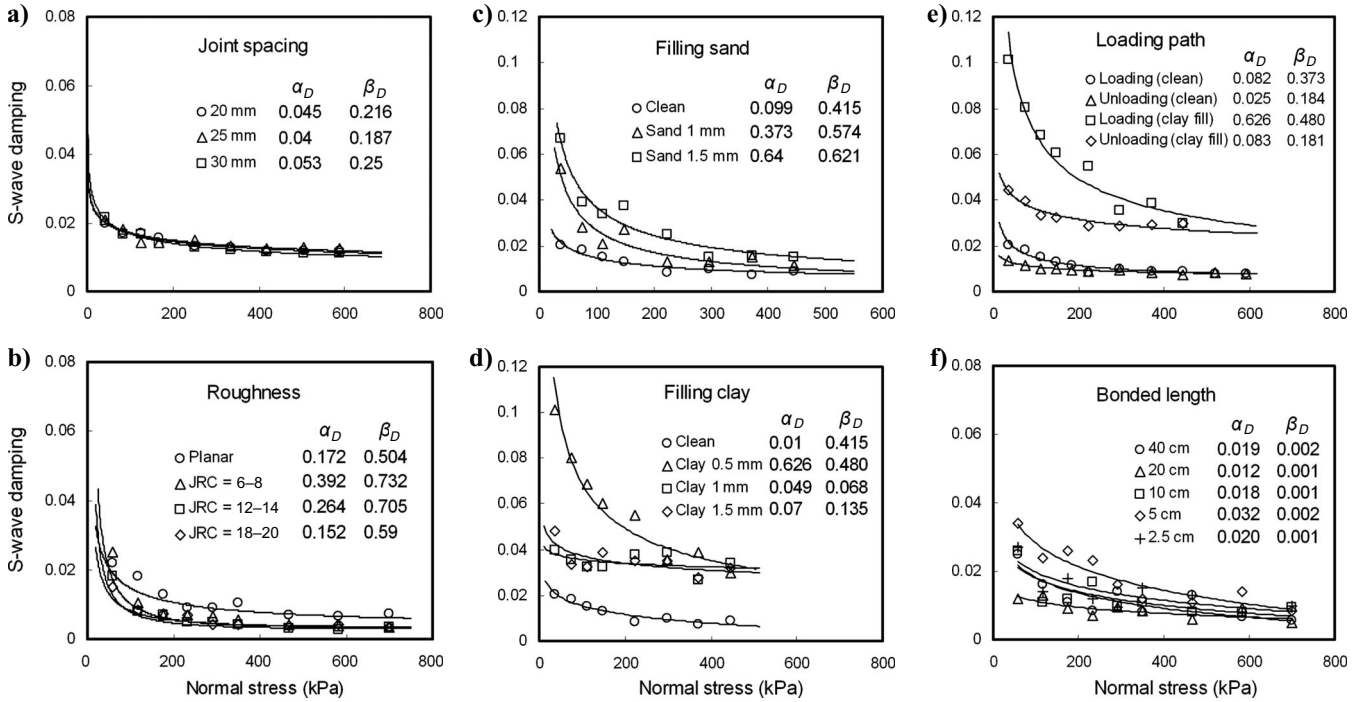

Figure 6. S-wave damping D_{rm} for different rock-mass conditions and stress levels: (a) effect of joint spacing (13 acetal discs, clean joints), (b) effect of joint roughness (15 dental gypsum discs), (c, d) effect of joint fillings (15 gneiss discs), (e) loading and unloading path (15 gneiss discs), and (f) effect of joint cementation (16 gypsum discs). The higher JRC value corresponds to rougher surfaces. "Sand 1 mm" stands for 1-mm-thick sand filling. The values for α_D (m/s) and β_D are the rock mass S-wave damping parameters in equation 8.

- *Joints filled with gouge material (Figure 6c and d):* The damping ratio increases in the presence of gouge material, particularly in thick joints filled with plastic fines.
- *Load history (Figure 6e):* Damping decreases in preloaded conditions.
- *Cemented joints (Figure 6f):* Although data resolution limits our ability to draw definitive conclusions, joint cementation appears to decrease losses and the stress sensitivity of attenuation.

ANALYSES: LONG-WAVELENGTH PROPAGATION IN JOINTED ROCKS

Velocity-stress trends

The strong influence of joint stiffness on the stiffness of a rock mass permits the application of Hertzian power functions to fit long-wavelength velocity versus normal stress data, analogous to wave propagation in soils (Hardin and Richart, 1963; Lee and Stokoe, 1986; Brady and Brown, 1995):

$$V_P = \alpha_P \left(\frac{\sigma_n}{1\ \text{kPa}} \right)^{\beta_P} \quad \text{and} \quad V_S = \alpha_S \left(\frac{\sigma_n}{1\ \text{kPa}} \right)^{\beta_S}. \qquad (3)$$

The factor α (m/s) is the wave velocity in the rock mass when $\sigma_n = 1$ kPa, and the exponent β describes the stress sensitivity of P- and S-wave velocities. The lines superimposed on data points in Figures 4 and 5 show the fitted equations; the corresponding α-β values are tabulated in each case. Figure 7 shows a plot of all the α-β pairs for P- and S-wave propagation; for comparison, the α-β pairs for the S-wave velocity in soils are shown in the same figure (data compiled from our laboratory experiments on a wide range of soils, from soft clays to dense sands). These results support several observations.

First, stress-dependent P- and S-wave velocity data gathered for jointed rock masses are well captured by the power functions in equation 3 (Figures 4 and 5). Second, there is an inverse relation between the α-factor and the β-exponent; in other words, a rock mass with high stiffness at low stress (i.e., a high α) is less sensitive to any increase in normal stress (i.e., a low β). Third, the S-wave α_S-β_S parameters for rock masses cluster above the trend for soils (Figure 7); hence, the wave velocity through the jointed rock masses is higher than in soils at the same state of stress. In agreement with $V_P > V_S$, the α_P-β_P pairs cluster above α_S-β_S.

In addition to the above points, the sequence of joint conditions in the order of decreasing β and increasing α is as follows: thick joints with plastic gouge, joints with nonplastic gouge and mismatched roughness, clean smooth joints, and cemented joints. Finally, preloaded jointed rocks have a higher α value and a lower β value than jointed rock masses during initial loading.

Interpretation of V_P/V_S

The ratio of longitudinal- to shear-wave velocities is related to the small-strain Poisson's ratio $\nu = -\varepsilon_\perp/\varepsilon_\parallel$ in homogeneous materials. However, this interpretation is unwarranted in the case of jointed rocks, where the strain parallel to loading $\varepsilon_\parallel$ and the transverse strain $\varepsilon_\perp$ are different in rock blocks and joints. Furthermore, the lateral deformation of the gouge material in the jointed rock column is restricted by friction against the rock block; the soft joint layer then acts with stiffness similar to the constrained modulus M rather than Young's modulus E during the axial excitation of the jointed column.

In an alternative approach, we explore the evolution of V_P/V_S versus normal stress as an indicator of the joint characteristics. The computed ratios are plotted in Figure 8. We note that the velocity ratio in rods can vary from $V_P/V_S \approx 1.41$ for a continuous rod with $\nu = 0$, to $V_P/V_S \to \infty$ for a jointed column with frictionless interfaces. The values of V_P/V_S in this study range from 2 to 3.6 for all hard block materials and from 1.7 to 2.4 for the soft acetal discs. We also note that the value of V_P/V_S remains constant when gneiss blocks are separated by clean planar joints. This response is consistent with Hertz-Mindlin contact behavior, where longitudinal and shear stiffness are determined by the contact area between the interacting surfaces (Figure 8a).

In addition, we note that when stiff block materials are involved, the value of V_P/V_S decreases as the normal stress increases in the case of the rough joints or joints with gouge material. The faster increase in shear stiffness than in longitudinal stiffness required for this V_P/V_S response corresponds to a granular model where the coordination number and rotational frustration increase during loading (Figure 8b). Finally, we note that the value of V_P/V_S increases as the normal stress increases and approaches the value for the intact block when soft acetal discs form the column; that is, the normal stiffness increases faster than the shear stiffness. Although a physical explanation remains unclear for this material, an idealized contact model is sketched in Figure 8c.

Joint properties from long-wavelength propagation measurements

Joint spring constant

The deformation of the rock mass in long-wavelength torsional or longitudinal excitation normal to joints is the sum of the rock and

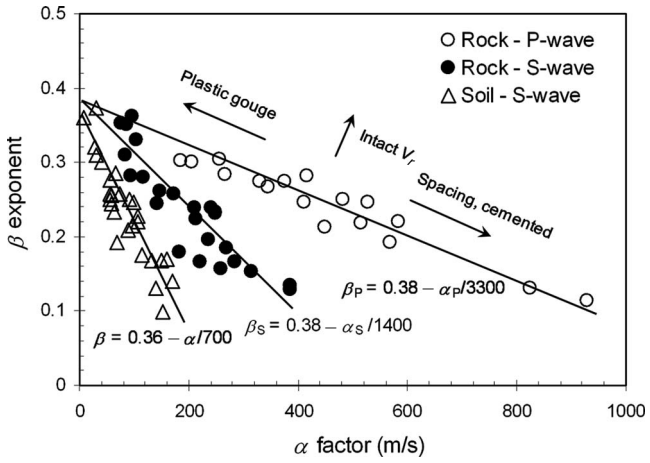

Figure 7. The rock-mass wave parameters of α versus β (equation 3) for various disc materials and joint conditions. For comparison, the data shown as open triangles were gathered for a wide range of soils, from high-plasticity clays to angular coarse sands, and the regression line of $\beta = 0.36 - \alpha/700$ applies to these soil data (from Santamarina et al., 2001). The variability for jointed rocks reflects the wide range of tested materials and conditions. The arrows highlight trends for selected variables.

joint deformation, i.e., a series system. In this case, the compliance of the rock mass combines joint and block compliances weighted by their lengths. This approach leads to the following expression for wave velocity in the rock mass V_{rm} (derivation in Fratta and Santamarina, 2002):

$$V_{rm} = \sqrt{\frac{1}{\rho_{rm}}\left(\frac{1-\eta}{V_r^2\rho_r} + \frac{\eta}{V_j^2\rho_j}\right)^{-1}}. \quad (4)$$

For P- and S-waves, ρ_{rm}, ρ_r, and ρ_j are the density of rock mass, intact rock, and joint, respectively; V_r and V_j are the velocity of the intact rock and joint, respectively; and η is the ratio of the joint thickness t to the interjoint spacing S, that is, $\eta = t/S$.

The application of this expression is hindered by the uncertainty in determining the effective thickness of the joints. The alternative is to consider the spring constant of the joints k_j (GPa/m) because it combines stiffness and thickness (Goodman, 1989). Let us adopt a power function for the spring constant in terms of the normal stress $k_j = \psi(\sigma/\text{kPa})^{\zeta}$ in agreement with contact mechanics (see also Brady and Brown, 1995), where the joint stiffness parameters ψ and ζ reflect the joint surface properties, the gouge type, the joint thickness, and the sensitivity to stress changes. The wave velocity in the rock mass can be computed in terms of the joint spring constant parameters and the separation between consecutive joints. Accordingly, we can express the wave velocity in the rock mass as

$$V_{rm} = \sqrt{\frac{1}{\rho_{rm}}\left(\frac{1}{V_r^2\rho_r} + \frac{1}{Sk_j}\right)^{-1}} = \sqrt{\frac{1}{\rho_{rm}}\left(\frac{1}{V_r^2\rho_r} + \frac{1}{S\psi\left(\frac{\sigma_n}{1\ \text{kPa}}\right)^{\zeta}}\right)^{-1}}. \quad (5)$$

Equation 5, which applies to P- and S-waves, enables us to determine the joint spring constant k_j or the stress-related joint parameters ψ and ζ from the macroscale wave propagation measurements in the rock mass. (Note that different stress levels are required to obtain $\psi - \zeta$. Furthermore, the mass density of the rock mass ρ_{rm}, the intact-rock wave velocity V_r, the intact-rock mass density ρ_r, and the interjoint separation S must be determined separately.) Equation 5 properly fits all velocity trends in Figures 4 and 5. An inverse relationship is observed between joint parameters ψ and ζ: Joints with low stiffness at low normal stress (i.e., low ψ) exhibit high sensitivity to the state of stress (i.e., high ζ). Exponents as high as $\zeta = 0.7$ to 0.8 are computed for joints filled with sand or clay. Changes in spacing do not affect ψ and ζ.

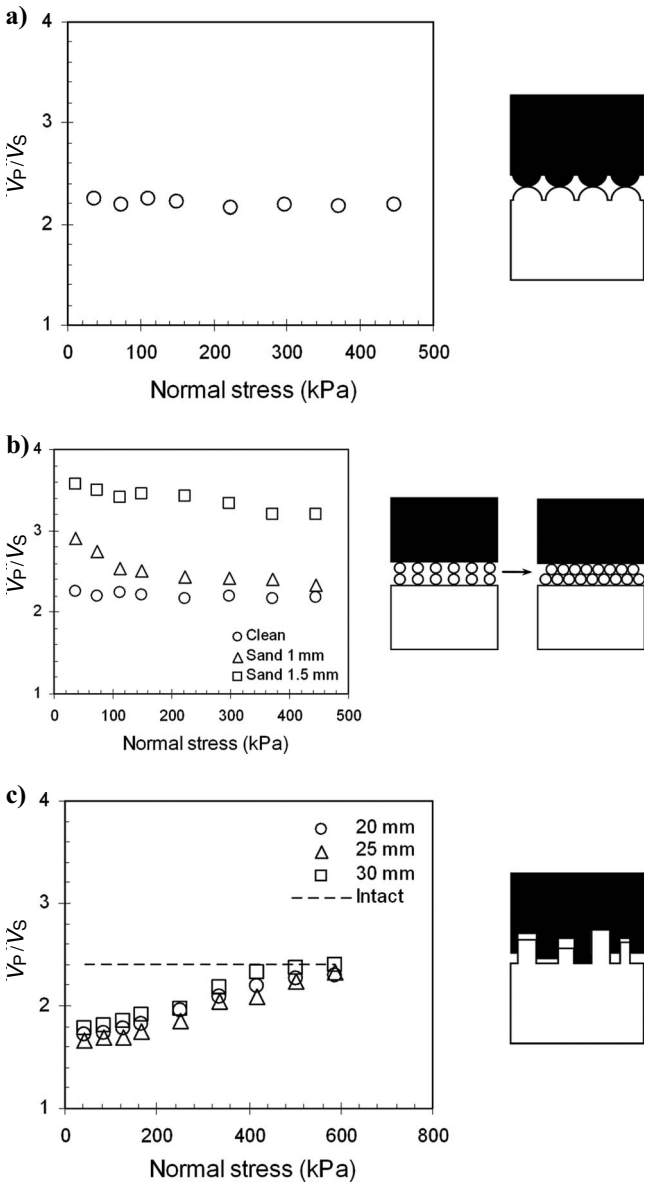

Figure 8. The V_P/V_S values for various joint properties and stress levels: (a) constant V_P/V_S (observed in column made of clean planar but stiff gneiss blocks), (b) decreasing V_P/V_S (observed in rock mass made of gneiss blocks with joint filling), and (c) increasing V_P/V_S (observed in column made of soft acetal discs).

Joint attenuation

Damping is the ratio between the energy lost per cycle ΔW and the stored energy W (Mavko et al., 1998). The energy lost in blocks and joints can be expressed in terms of their corresponding damping ratios and stiffness. In many field applications as well as for the parameter range tested in this study, rock mass damping is controlled by losses in the joints $D_{rm} \approx D_j$. If the frictional loss in joints is the principal attenuation mechanism, then the hysteretic damping can be computed assuming a hyperbolic stress-strain response (Duncan and Chang, 1970; Fratta and Santamarina, 2002):

$$D_{rm} = D_j = \frac{2}{3\pi}\gamma_j\frac{G_j}{\tau_{ult}}, \quad (6)$$

where the joint shear modulus G_j is related to the joint stiffness k_j as $G_j = k_j t$, the joint stiffness k_j is a power function of the normal stress, and the shear strength τ_{ult} depends on the normal stress according to Coulomb's law, $\tau_{ult} = \sigma_n \tan\phi$ (where ϕ is the friction angle).

Equation 6 then becomes

$$D_{rm} \approx D_j = \left(\frac{2}{3\pi}\frac{\psi t}{\tan\phi}\gamma_j\right)\left(\frac{\sigma_n}{1\ \text{kPa}}\right)^{-1+\zeta} = \alpha_D\left(\frac{\sigma_n}{1\ \text{kPa}}\right)^{-\beta_D}. \quad (7)$$

A power function is obtained once again; however, in this case, the joint attenuation parameter α_D is strain dependent, or $\alpha_D = f(\gamma_j)$. The negative exponent indicates that the damping ratio is expected to decrease as the normal stress increases, in agreement with experimental results presented in Figure 6, where the lines show the fitted trend. Attenuation parameters α_D-β_D are tabulated in each case.

CONCLUSIONS

In this study, we have investigated the stress-dependent propagation characteristics in jointed rock masses. Long-wavelength data were gathered using a jointed-column device that helped us explore the effects of various joint conditions on P- and S-wave propagation while we controlled the stress normal to joints.

Data obtained under well-controlled laboratory conditions show that P- and S-wave velocities increase and attenuation decreases as the normal stress increases. The presence of gouge material, particularly if the material is of clay origin, lowers the propagation velocity and increases attenuation. A higher level of rock-mass stiffness is attained with well-matched grooved surfaces than with mismatched rough surfaces. At a given normal stress, jointed rock masses retain memory of the loading history, and the wave velocity is higher during unloading than during loading in most cases. The memory is associated with changes in asperities on the faces of joints and in the gouge material. Joint cementation effectively increases wave velocity through the rock mass and decreases its stress sensitivity.

Stress-dependent P- and S-wave velocity data gathered for jointed rock masses are well captured by the power function of contact mechanics, $V = \alpha\sigma^{\beta}$. There is an inverse relation between the α-factor and the β-exponent; hence, a rock mass with high stiffness at low stress (i.e., high α) is less sensitive to the increase in normal stress (i.e., low β). In order of decreasing β parameters and increasing α parameters, the joint conditions vary as follows: thick joints with plastic gouge, joints with nonplastic gouge and mismatched roughness, clean smooth joints, and cemented joints. Preloaded jointed rocks have a higher α value and a lower β value than jointed rock masses during first loading.

The measured V_P/V_S values vary between 2 and 3.6 for jointed columns made of hard blocks. The interpretation of V_P/V_S in terms of Poisson's ratio is unwarranted in the case of jointed rocks. Instead, the evolution of V_P/V_S during changes in the normal stress reflects joint characteristics and stress response.

Displacements concentrate at joints. The assumption of frictional loss at joints leads to a power law between damping and normal stress with a negative exponent.

Effective media equations can be fitted to stress-dependent velocity or attenuation data to recover joint information such as the joint spring constant k_j (or joint parameters ψ and ζ) and damping D_j.

Taken together, the rock mass parameters of α-β (for P-wave and S-wave velocity and damping), the changes in V_P/V_S with normal stress, and the joint parameters k_j and D_j provide insightful information about the rock mass and the characteristics of joints. Hence, seismic measurements can be used to augment rock mass characterization in engineering applications.

ACKNOWLEDGMENTS

This work was supported by the Korea Research Foundation Grant, funded by the Korean Government (MOEHRD) (KRF-2007-313-D00801).

REFERENCES

Barton, N. R., and V. Choubey, 1977, The shear strength of rock joints in theory and practice: Rock Mechanics and Rock Engineering, **10**, 1–54.
Boadu, F. K., 1997, Fractured rock mass characterization parameters and seismic properties: Analytical studies: Journal of Applied Geophysics, **36**, 1–19.
Boadu, F. K., and T. L. Long, 1996, Effects of fractures on seismic wave velocity and attenuation: Geophysical Journal International, **127**, 86–110.
Brady, B. H. G., and E. T. Brown, 1995, Rock mechanics: For underground mining: Chapman and Hall.
Brillouin, L., 1946, Wave propagation in periodic structures: McGraw-Hill Book Co.
Duncan, J. M., and C. Y. Chang, 1970, Nonlinear analysis of stress and strain in soils: Journal of Soil Mechanics and Foundation Division, **96**, 1629–1653.
El-Naqa, A., 1996, Assessment of geomechanical characterization of a rock mass using a seismic geophysical technique: Geotechnical and Geological Engineering, **14**, 291–305.
Fratta, D., and J. C. Santamarina, 2002, Shear wave propagation in jointed rock: State of stress: Géotechnique, **52**, 495–505.
Goodman, R. E., 1989, Introduction to rock mechanics, 2nd ed.: John Wiley & Sons, Inc.
Guéguen, Y., and V. Palciauskus, 1994, Introduction to the physics of rock: Princeton University Press.
Hardin, B. O., and F. E. Richart, 1963, Elastic wave velocities in granular soils: Journal of Soil Mechanics and Foundation Division, **89**, 33–65.
Huang, T. H., C. S. Chang, and Z. Y. Yang, 1995, Elastic moduli for fractured rock mass: Rock Mechanics and Rock Engineering, **28**, 135–144.
Kahraman, S., 2001, A correlation between P-wave velocity, number of joints and Schmidt hammer rebound number: International Journal of Rock Mechanics and Mining Sciences, **38**, 729–733.
———, 2002, The effects of fracture roughness on P-wave velocity: Engineering Geology, **63**, 347–350.
Kikuchi, K., T. Igari, Y. Mito, and S. Utsuki, 1997, In situ experimental studies on improvement of rock masses by grouting treatment: International Journal of Rock Mechanics and Mining Sciences, **34**, 138.e1–138.e14.
Kolsky, H., 1963, Stress waves in solids: Dover Publ. Inc.
Lee, S. H. H., and K. H. Stokoe II, 1986, Investigation of low-amplitude shear wave velocity in anisotropic material: University of Texas, Austin, Civil Engineering Department Report GR86-06.
Leucci, G., and L. De Giorgi, 2006, Experimental studies on the effects of fracture on the P and S wave velocity propagation in sedimentary rock ("Calcarenite del Salento"): Engineering Geology, **84**, 130–142.
Mavko, G., T. Mukerji, and J. Dvorkin, 1998, The rock physics handbook: Cambridge University Press.
Priest, S. D., 1993, Discontinuity analysis for rock engineering: Chapman and Hall.
Pyrak-Nolte, L. U., L. R. Myer, and N. G. Cook, 1990a, Transmission of seismic wave across single natural fracture: Journal of Geophysical Research, **95**, 8617–8638.
———, 1990b, Anisotropy in seismic velocities and amplitudes from multiple parallel fractures: Journal of Geophysical Research, **95**, 11345–11358.
Santamarina, J. C., K. A. Klein, and M. A. Fam, 2001, Soils and waves: John Wiley & Sons, Inc.
Schoenberg, M., and F. Muir, 1989, A calculus for finely layered anisotropic media: Geophysics, **54**, 581–589.
Schoenberg, M., and C. M. Sayers, 1995, Seismic anisotropy of fractured rock: Geophysics, **60**, 204–211.
Sjogren, B., A. Ofsthus, and J. Sandberg, 1979, Seismic classification of rock

mass qualities: Geophysical Prospecting, **27**, 409–442.
White, J. E., 1983, Underground sound: Application of seismic waves: Elsevier Science Publ. Co., Inc.
Yi, W., K. T. Nihei, J. W. Rector, S. Nakagawa, L. R. Myer, and N. G. W. Cook, 1997, Frequency-dependent seismic anisotropy in fractured rock: International Journal of Rock Mechanics and Mining Sciences, **34**, paper 349.
Zhao, J., X. B. Zhao, and J. G. Cai, 2006, A further study of P-wave attenuation across parallel fractures with linear deformational behavior: International Journal of Rock Mechanics and Mining Sciences, **43**, 776–788.